Publication status: This preprint has not been published elsewhere.

Validation of SWOT significant wave height against in situ and model observations on the northeastern Brazilian continental shelf

Yuri Onça Prestes, Alex Costa Silva, Ramilla Vieira de Assunção, Gabriel D'annunzio Gomes Junior, Marcus Silva, Aouf Lotfi, Angelo Lemos, Fabrice Hernandez

https://doi.org/10.1590/2675-2824074.25257

Submitted on: 2026-07-30
Posted on: 2026-08-03 (version 1)
(YYYY-MM-DD)

Ocean and Coastal Research

http://dx.doi.org//10.1590/2675-2824074.25257

ISSN 2675-2824

Validation of SWOT significant wave height against in situ and model observations on the northeastern Brazilian continental shelf

PRESTES, Y. O.[1]; SILVA, A. C.[1]; ASSUNÇÃO, R. V.[1]; GOMES, G. D.[1]; SILVA, M. A [1]; LOTFI, A.[2]; LEMOS, A.T.[3]; HERNANDEZ, F.[4]

Y.O.P.: https://orcid.org/0000-0002-2065-8403

A.C.S.: https://orcid.org/0000-0002-5828-3598

R.V.A.: https://orcid.org/0009-0000-4011-3657

G.D.G.: https://orcid.org/0000-0001-8969-3605

M.A.S.: https://orcid.org/0000-0001-9749-6644

L.A.: https://orcid.org/0000-0002-0279-6773

A.T.L.: https://orcid.org/0000-0003-1229-9807

F.H.: https://orcid.org/0000-0003-2152-0657

[1] Laboratório de Oceanografia Física Estuarina e Costeira, Departamento de Oceanografia, Universidade Federal de Pernambuco, Recife, Pernambuco, Brazil
[2] Centre National de Recherches Météorologiques, Toulouse, France
[3] Environmental Sciences Center, Federal University of Southern Bahia, Itabuna 45600-923, Brazil
[4]Laboratoire d'Études en Géophysique et Océanographie Spatiales, Institut de Recherche pour le Développement et Université de Toulouse, Toulouse, France

* Corresponding author: yo.prestes@gmail.com

Abstract

The ability of the SWOT (Surface Water and Ocean Topography) satellite-derived significant wave height (SWH) estimates to represent conditions on the continental shelf of the Abrolhos Archipelago was assessed using an AWAC as the reference dataset; WAVEWATCH-III (WW3) was used as an auxiliary numerical field for spatial context. By collocating observations in space and time and applying standard statistical metrics, a high consistency between SWOT and AWAC was revealed (R ≈ 0.90; RMSE ≈ 0.25 m), with a small positive mean bias. Agreement with WW3 was likewise robust (R ≈ 0.88), indicating that the wave patterns observed by SWOT are physically consistent with the broader regional wave field represented by the numerical model. SWOT adequately represented temporal variability (including higher-energy events), although a slight overestimation tendency was detected. Overall, these findings indicate that SWOT-derived SWH reliably represents wave dynamics on the continental shelf when evaluated against in situ observations. The agreement with WW3 further supports the regional coherence of the satellite-derived wave field, reinforcing its applicability to coastal studies.

Keywords: SWOT; Altimetry; Significant wave height; Remote sensing.

INTRODUCTION

Surface waves are regarded as central agents in the transfer of momentum, energy, and sediments across continental shelves, and they strongly influence coastal processes such as sediment transport, erosion, and connectivity among marine habitats; therefore, precise characterization of significant wave height (SWH) and spectral parameters is essential for physical studies and coastal applications (Mahadevan, 2016; Queffeulou, 2004). Satellite observational products complement point-based networks (e.g., buoys) by providing broad spatial coverage (Timmermans et al., 2020); however, their accuracy is known to vary near the coast due to footprint effects, retracking issues, and inherent differences across time and space (Fu and Ubelmann, 2014; Zhang et al., 2024). Swath altimeters, including the SWOT (Surface Water and Ocean Topography) satellite mission, enhance the two-dimensional observational capability of the sea surface, providing new opportunities for mapping wave variability, with direct implications for swell monitoring and the evaluation of numerical wave models.

By combining the KaRIn interferometer with a complementary nadir altimeter, the SWOT mission provides imagery that enables the detection of surface signals with unprecedented spatial resolution, including long-period swells and coastal-scale variability that conventional nadir altimeters do not readily resolve (López-García et al., 2019; Wang and Fu, 2019; Ardhuin et al., 2024; Zhang et al., 2024). Initial studies have shown that SWOT can detect swells and estimate SWH under favorable conditions; consequently, it is a promising tool for validating and complementing in-situ measurements and model products (Wang et al., 2018; Ardhuin et al., 2024; Turki et al., 2025). However, the literature also highlights challenges related to swath sensitivity, product type (high-rate versus low-rate), and the need for local calibration/validation to ensure confidence and quality of results in coastal zones (Fu and Ubelmann, 2014). The objective of the present study is to evaluate SWOT-derived SWH against AWAC buoy observations, while using WAVEWATCH III (WW3) as an auxiliary dataset to assess the spatial coherence of the observed wave field. Therefore, including WW3 in the analysis provides an auxiliary numerical field to support the spatial interpretation of the wave pattern and complement the local AWAC observations, without serving as an independent validation benchmark for SWOT-derived SWH.

Previous validations of altimetric SWH and multi-mission products have revealed that metrics such as RMSE, bias, and correlation are strongly dependent on regional factors (e.g., wind conditions, presence of remote swells, and the spectral representation of the wave field), and that global models display limitations at coastal scales that can be mitigated by regional high-resolution grids and/or data assimilation. For next-generation altimeters, when spatial and temporal collocation are adequate, very high correlations between satellite and in-situ sensors can be obtained, although systematic biases and pointwise dispersion remain central issues to be addressed in subsequent studies (Queffeulou, 2004; Ardhuin et al., 2024). Hence, regional investigations such as the present one are essential to assess the practical usefulness of the SWOT product on continental shelves and to guide improvements in products and validation methodologies.

The manuscript is organized as follows: Section 2 describes the methods and datasets used in the present study (SWOT products, observational data, and model outputs), the spatial/temporal collocation criteria, and the statistical metrics applied; Section 3 presents temporal and spatial comparisons among the three datasets; Section 4 discusses the observed differences, possible error sources, and relates the findings to the literature. Finally, Section 5 presents the main conclusions of the study.

METHODS

Study Area

The mooring from which the in-situ data were collected was located on the northeastern Brazilian continental shelf (Figure 1), near the Abrolhos Archipelago, approximately 70 km off the southern coast of the state of Bahia, Brazil. This region is part of a continental shelf more than 240 km wide (Knoppers et al., 1999). The Abrolhos Archipelago comprises five volcanic islands and is part of the Abrolhos Marine National Park, an area of high biodiversity colonized by coral reefs and recognized as a breeding ground for humpback whales (ICMBio, 2018; Morete et al., 2022).

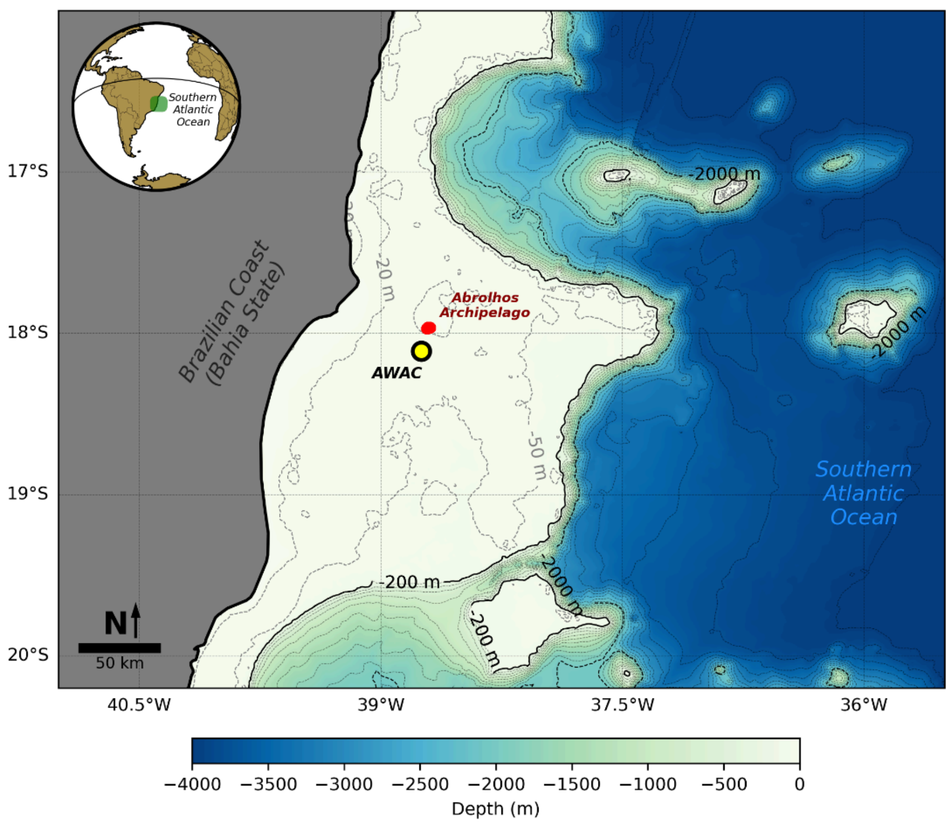

Figure 1. Map of the study area in the South Atlantic Ocean. The Brazilian coastline is shown, specifically the southern coast of the state of Bahia. The yellow circle indicates the location of the AWAC wave-buoy mooring on the continental shelf.

The wind regime during this time of year is predominantly from the south and southeast, associated with storm-related winds, with a monthly mean magnitude of approximately 7.0 m s^{-1} between May and July (Lessa and Cirano, 2006). Wind stress is a critical forcing mechanism for subinertial currents parallel to the coast, driven by northeasterly winds, and this is considered the primary factor of coastal flow on the continental shelf (Teixeira et al., 2013). Another mechanism generating cross-shelf currents is the semidiurnal tide, which reaches approximately 0.5 m s^{-1} under a mesotidal regime, with tidal amplitudes less than 3.0 m (Castro et al., 2013). According to the literature, the mean wave direction during the sampling period is from the southeast (Contrim et al., 2022). The highest waves (> 4 m) are observed in winter, reaching up to 4.9 m with a southwest direction (Pianca et al., 2010).

The SWOT Satellite

The SWOT satellite, a joint mission of NASA and CNES with participation from CSA and UKSA, is employed to map the topography of oceanic and continental water surfaces at unprecedented resolution. Its primary instrument, the Ka-band Radar Interferometer (KaRIn), performs two-dimensional measurements of sea level across two lateral swaths (each ≈ 50–60 km, totaling ≈ 120 km of swath), with an effective spatial resolution that allows for the observation of structures down to ≈ 15 km (Fu and Ubelmann, 2014). This approach increases the detection capability of conventional altimetry by roughly an order of magnitude, allowing small-scale ocean features (such as submesoscale vortices, fronts, and internal waves) to be observed, which is relevant to vertical mixing processes and to the redistribution of heat, carbon, and nutrients (Mahadevan, 2016). Furthermore, recent evidence indicates that SWOT can detect long-period swells and estimate SWH under certain conditions (Ardhuin et al., 2024).

During the initial Cal/Val phase, rapid revisits were conducted to characterize high-frequency processes and to support calibration and validation of the orbital products; after this phase, the mission entered nominal orbit operations with a 21-day repeat cycle, covering latitudes roughly between 78°N and 78°S (Wang et al., 2018; Wang and Fu, 2019). In addition, a nadir altimeter (POSEIDON-3C) is carried onboard and provides nadir measurements that complement the KaRIn maps and are frequently used in joint calibration/validation routines (Guérin et al., 2024). Due to variations in sensitivity across the swath, product type (high-rate vs low-rate), and the geophysical corrections required, local validation with buoys/moorings is recommended, and caution is advised when interpreting coastal and very small-scale signals (SWOT Science Team, 2024; Zhang et al., 2024).

The SWOT data used in this study correspond to the dataset-l2-swot-karin-lr-ssh-validated/WindWave product, provided through the ODATIS/AVISO Altimetry data portal. These data are Level-2 low-resolution (L2 LR) products generated with the initial PIC0 algorithm, as the analyzed period predates the later PIC2 and PID0 updates. No quality filter was applied by the product provider; instead, the data were further screened in this study using tolerance thresholds on SWH and sigma0 before the collocation analysis.

In situ observations

The in-situ measurements were obtained from an AWAC ADCP (600 kHz), manufactured by NORTEK, deployed on the northeastern Brazilian continental shelf near the Abrolhos Archipelago, at coordinates 38°45.14′ W and 18°6.72′ S (Figure 1). The instrument was installed at a water depth of approximately 30 m and positioned about 21.5 m below the sea surface, corresponding to approximately 8.5 m above the seabed. The AWAC was deployed in autonomous mode and powered by an external battery pack. Wave measurements were acquired every hour using bursts of 2048 samples recorded at 1.0 Hz, resulting in 2048 s (34.1 min) acquisition windows. The compass update rate was 1800 s, and the coordinate system was ENU. The wave bursts were processed following standard manufacturer procedures, including quality control based on signal correlation, amplitude, and signal-to-noise ratio, with removal of spikes and exclusion of low-quality ensembles. The mean water-level signal was removed before spectral analysis, and a Hanning window was applied prior to FFT processing to reduce spectral leakage. The resulting wave spectrum was used to estimate SWH and other integral wave parameters.

Global Model

WW3 is a third-generation spectral numerical model developed by the National Centers for Environmental Prediction (NCEP/NOAA) (Tolman, 1997; Tolman, 1999a; Tolman, 2002; Tolman, 2009) and is the direct successor of the WaveWatch (Tolman, 1989; Tolman, 1991) and WAVEWATCH II (Tolman, 1992) models. However, WAVEWATCH III presents significant differences relative to its predecessors, encompassing key aspects such as the governing equations, model architecture, numerical techniques, and parameterizations of physical processes. The model solves the spectral action density balance equation using a finite-difference scheme in an Eulerian formulation and incorporates ice-cover effects. To avoid loss of spectral resolution in shallow waters, the model applies modified versions of its basic equations, incorporating the kinematic changes in wavenumber associated with shoaling. More recent versions offer greater computational flexibility by including options for curvilinear and unstructured grids, unlike earlier versions that were restricted to regular grids.

The WW3 model has been widely used for validation and comparison with altimeter, buoy, and ADCP measurements. In the present study, WW3 was used as an auxiliary numerical dataset to provide spatial context for the wave field over the study region and to assess the physical consistency of the wave patterns observed by SWOT relative to the local AWAC measurements. Therefore, WW3 was not treated as an independent validation reference. In global and regional applications, the model is typically configured with spectral discretization of approximately 24 directions and 25–30 frequency bands, running on grids of 0.25°–0.5° (~25–50 km) and forced by 10 m winds from reanalyses or forecasts. WW3 is extensively employed in operational systems as well as in long-term studies. The Hydrography Center of the Brazilian Navy (CHM) runs global WW3 versions forced by GFS and ICON winds to provide wave boundary conditions for the South Atlantic (Marinha do Brasil, 2025), while the University of Hawaii maintains a global model (~0.5° resolution) with seven-day forecasts for ocean applications (NOAA, 2023). More recently, the availability of high–spatial resolution measurements from the SWOT mission has enabled comparisons between WW3-modeled SWH and satellite observations as well as in-situ sensors, such as the AWAC wave gauge used in the present study, moored near the Abrolhos Archipelago (Figure 1).

The WW3 configuration employed in this study corresponds to the operational wave-forecast system that feeds the SurfGuru platform. The model was configured using three nested grids along the Brazilian coast: the Global grid (0.5° × 0.5°), the Brazil grid (0.25° × 0.25°), and the Coastal grid (0.0625° × 0.0625°), with the results analyzed here corresponding to the Coastal grid. The model was forced by 10 m winds from the Global Forecast System (GFS) with 0.25° × 0.25° spatial resolution and 3-hour resolution, and the model outputs also have 3-hour temporal resolution. The spectral discretization consisted of 25 frequency bins and 24 directional sectors (15°). The physical parameterizations included BT1 and LRB4 bottom-friction schemes, and neither currents nor tides were included in the simulations. Because no dedicated validation study is available for this exact configuration, it is used to complement the analysis through comparison with AWAC observations and SWOT measurements, without being independently validated in this study.

Statistical analyses

The WW3 time series was extracted at a grid point located approximately 16 m from the AWAC mooring site (38°45.14′ W, 18°6.72′ S), while the SWOT SWH time series was obtained from satellite overpasses within 20 km of the mooring. After assembling the three datasets to ensure spatial agreement, the simultaneous time frame was identified between 2 June and 9 July 2023. Daily mean SWH values were then computed for the comparison of the time series. The use of daily mean values was adopted to ensure temporal consistency among the datasets, given the intermittent nature of SWOT overpasses compared to the continuous records provided by the AWAC and WW3 datasets. This approach reduces the influence of high-frequency variability (e.g., hourly fluctuations) and minimizes potential mismatches associated with nearest-time collocation. Although this averaging may smooth short-term variability, it provides a more robust basis for comparison across datasets with different temporal sampling characteristics, as commonly applied in satellite validation studies. Future analyses could explore higher-frequency collocation approaches to further assess short-term variability.

In addition to the daily means, basic descriptive statistics were calculated for each time series, including mean, median, standard deviation, variance, minimum and maximum values, range, and coefficient of variation. To assess the agreement among the SWH time series, correlation metrics, linear regression, and error statistics were applied. Pearson's correlation coefficient (r), which quantifies the linear association between two variables, was estimated as follows:

$$r = \frac{\sum_{i=1}^{n}\left(x_i - \bar{x}\right)\left(y_i - \bar{y}\right)}{\sqrt{\sum_{i=1}^{n}\left(x_i - \bar{x}\right)^2 \sum_{i=1}^{n}\left(y_i - \bar{y}\right)^2}} \quad \text{(Eq. 1)}$$

where x_i denotes the SWOT SWH anomaly at time i, while x_i represents the corresponding anomaly from the observational series or from the global wave model.

Since the relationship between two series may not be strictly linear, the analysis was complemented by the non-parametric Spearman correlation (ρ), which is suitable for identifying monotonic associations between the variables. This metric, based on the ranking of the observations, was computed as follows:

$$\rho = 1 - \frac{6\sum d_i^2}{n(n-1)} \quad \text{(Eq. 2)}$$

where d_i is the difference between the ranks of x_i and y_i.

Monotonic agreement was also assessed using Kendall's τ coefficient, defined as follows:

$$\tau = \frac{N_c - N_d}{\frac{1}{2}n(n-1)} \quad \text{(Eq. 3)}$$

where N_c and N_d correspond to the numbers of concordant and discordant pairs, respectively.

The quality of the linear fit between the series was quantified using the coefficient of determination R^2:

$$R^2 = 1 - \frac{\Sigma\left(y_i - \hat{y}_i\right)^2}{\Sigma\left(y_i - \bar{y}\right)^2} \quad \text{(Eq. 4)}$$

In addition to the slope and intercept of the simple linear regression, error magnitudes were evaluated using RMSE, MAE, and Bias. The statistical significance of all correlation coefficients was assessed through the associated p-value, considering a 95% confidence level ($p < 0.05$) as the reference.

The statistical distribution of SWH values was examined using normalized histograms, which were fitted with the Gumbel extreme-value distribution. For each dataset (SWOT, AWAC, and WW3), the location (loc) and scale (scale) parameters were estimated by maximum likelihood, and the Gumbel probability density function was computed as:

$$f(x) = \frac{1}{\beta} exp\left[- z - e^{-z}\right], \; z = \frac{x - \mu}{\beta} \quad \text{(Eq. 5)}$$

where the parameter μ represents the location parameter (loc), β the dispersion parameter (scale), and z denotes the reduced, dimensionless variable (the SWH value centered on μ and scaled by β). The theoretical mean of the distribution involves the Euler–Mascheroni constant $\gamma \approx 0.5772$, which naturally arises in the analytical solutions associated with the extreme-value distribution and is related to the shape of the Gumbel tail. In addition, a non-parametric Kernel Density Estimate (KDE) was also included to complement the empirical characterization of the observed distributions.

RESULTS

SWH TIME SERIES AND BASIC STATISTICS

The daily mean SWH values for the SWOT, AWAC, and WW3 datasets are presented in Figure 2. Visual agreement among the curves from the three datasets is evident. An oscillation with an approximate 5-day period can be identified throughout the series. The SWOT, AWAC, and WW3 curves similarly represented the maximum and minimum variations in SWH, for example, on 8 June and 3 July (Figure 2). It was also observed that the SWOT SWH values were higher than those from AWAC and WW3 during nearly the entire time series.

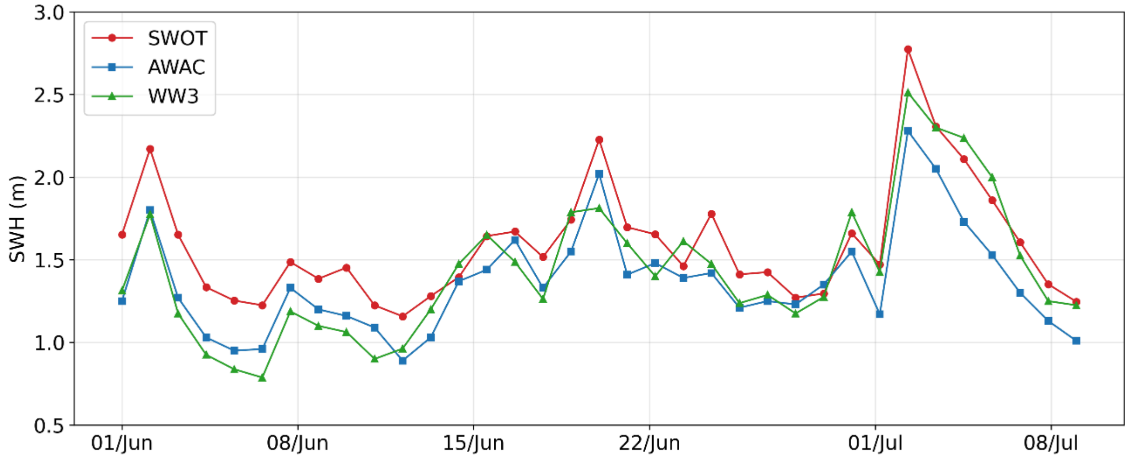

Figure 2. Time series of daily mean SWH derived from the SWOT satellite, the AWAC mooring, and the global WW3 model. The period shown spans from 1 June to 9 July 2023.

The visual comparison of the curves is informative but not sufficient. Therefore, basic statistics were computed for the time series of the three datasets (Table 1). The basic SWH statistics reveal consistent differences among the three sources analyzed. SWOT presented the highest mean (1.59 m) and median (1.49 m), indicating systematically higher wave levels compared with AWAC, which showed a mean of 1.36 m and a median of 1.33 m. WW3 exhibited intermediate values (mean of 1.42 m; median of 1.31 m), but displayed the largest dispersion, with a standard deviation of 0.41 m and a variance of 0.16, compared with 0.35 m / 0.12 m^2 for SWOT and 0.31 m / 0.10 m^2 for AWAC. The range confirmed this greater variability in the model, reaching 1.72 m in WW3, followed by 1.61 m in SWOT and 1.39 m in AWAC. The coefficient of variation reinforced this pattern, reaching 28.7% in WW3, while SWOT and AWAC remained similar (22.5% and 23.4%, respectively). Taken together, these results show that SWOT reproduces SWH values close to those observed by AWAC, whereas WW3 exhibits a greater spread.

Table 1. Basic statistics of the along-track SWH, including mean, median, standard deviation, variance, minimum, maximum, range, and coefficient of variation. Units are given for each metric.

Basic statistics	SWOT	AWAC	WW3
Mean (m)	1.59	1.36	1.42
Median (m)	1.48	1.33	1.31
Standard Deviation (m)	0.35	0.31	0.41
Variance (m^2)	0.12	0.10	0.16
Minimum (m)	1.15	0.89	0.78
Maximum (m)	2.77	2.28	2.51
Range (m)	1.61	1.39	1.72
Coefficient of Variation (%)	22.5	23.4	28.7

The histograms (Figure 3), together with the Gumbel fits, reinforce the conclusions drawn from the basic statistics: all series exhibit positive skewness and a modal peak around 1.2–1.4 m, with the SWOT distribution shifted toward slightly higher values. The fitted Gumbel parameters were (loc, scale) ≈ (1.44, 0.24) for SWOT, (1.22, 0.24) for AWAC, and (1.24, 0.32) for WW3. Using the theoretical Gumbel relation for the mean, μ_{Gumbel} = loc + γ·scale (com γ≈0.57), the predicted means are 1.59 m (SWOT), 1.36 m (AWAC), and 1.42 m (WW3), in excellent agreement with the empirical means shown in Table 1. The larger scale parameter obtained for WW3 (scale ≈ 0.32) indicates a more pronounced right tail and greater dispersion, consistent with the higher standard deviation observed for WW3 in the basic statistics. Overall, the Gumbel modeling visually and numerically confirms that SWOT tends to register slightly higher mean levels, AWAC provides the most centered distribution, and WW3 exhibits greater variability and a more elongated tail.

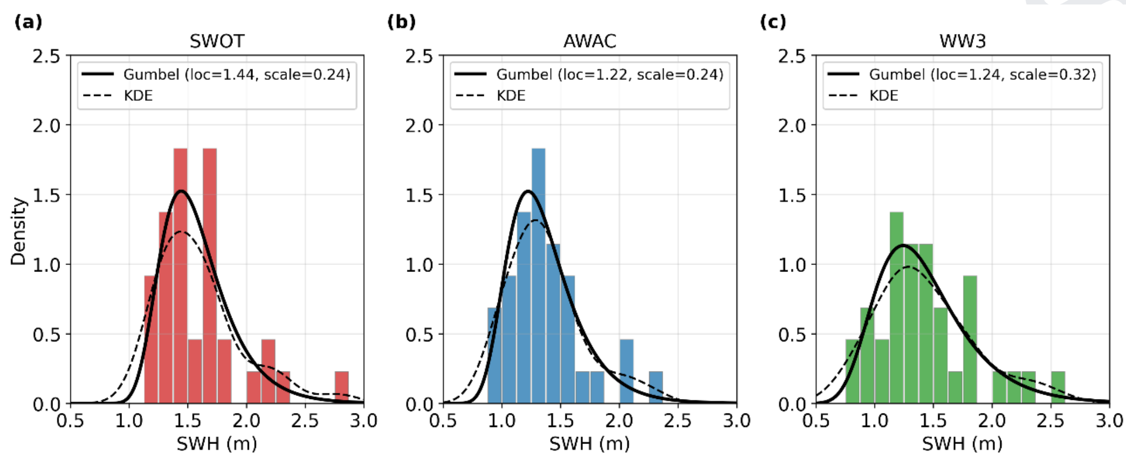

Figure 3. Normalized histograms of SWH for (a) SWOT, (b) AWAC, and (c) WW3. The black line represents the fitted Gumbel probability density function (PDF), and the dashed grey line shows the non-parametric kernel density estimate (KDE).

Validation Statistics and Performance

The results show strong agreement between SWOT and AWAC, indicating good performance of the satellite product relative to the in situ reference (Table 2). The Pearson correlation coefficients were 0.94 for SWOT versus AWAC, 0.88 for SWOT versus WW3, and 0.90 for AWAC versus WW3. The non-parametric correlations showed the same pattern, with Spearman values of 0.90, 0.85, and 0.89, and Kendall's tau values of 0.75, 0.68, and 0.73, respectively, all highly significant. The linear regression slopes were close to one for the SWOT–AWAC and SWOT–WW3 comparisons (1.06 and 1.01, respectively), while the AWAC–WW3 comparison showed a slope of 1.16. Among the pairwise comparisons, SWOT–AWAC showed the highest coefficient of determination (R^2 = 0.89), indicating that the linear relationship effectively explains the observed variability in that pair.

Table 2. Correlation coefficients (Pearson, Spearman, Kendall), linear regression parameters (slope and intercept), goodness-of-fit (R^2), and error metrics (RMSE, MAE, and Bias). The statistical significance (p-values) associated with each correlation metric is also included.

Metrics	SWOT vs AWAC	SWOT vs WW3	AWAC vs WW3
Pearson correlation coefficient	0.94	0.88	0.90
p-value (Pearson)	1.34×10^{-17}	8.79×10^{-13}	9.84×10^{-14}
Spearman rank correlation	0.90	0.85	0.89
p-value (Spearman)	5.98×10^{-14}	3.83×10^{-11}	2.01×10^{-13}
Kendall's tau	0.75	0.68	0.73
p-value (Kendall)	1.62×10^{-10}	6.79×10^{-9}	4.85×10^{-10}
Regression slope	1.06	1.01	1.16
Regression intercept (m)	0.14	–0.19	–0.15
R^2	0.89	0.79	0.81
RMSE (m)	0.25	0.24	0.19
MAE (m)	0.2338	0.2052	0.1589
Bias (a–b) (m)	–0.2307	0.1666	–0.0641
Normalized mean bias (%)	–16.90	10.44	–4.70

Among the absolute errors, the SWOT–AWAC comparison yielded RMSE = 0.25 m, MAE = 0.2338 m, and Bias = –0.2307 m, indicating a slight underestimation by SWOT relative to AWAC. The SWOT–WW3 comparison resulted in RMSE = 0.24 m, MAE = 0.2052 m, and Bias = +0.1666 m, indicating a slight overestimation by SWOT relative to WW3. For the AWAC–WW3 comparison, the error statistics were RMSE = 0.19 m, MAE = 0.1589 m, and Bias = –0.0641 m, showing the smallest absolute differences among the three pairwise analyses. Overall, the results demonstrate strong consistency between SWOT and the AWAC observations, supporting the reliability of the satellite-derived SWH. In addition, the agreement between SWOT and WW3 suggests that the spatial patterns observed by SWOT are physically consistent with the broader wave field represented by the numerical model.

Figure 4 directly illustrates the statistical relationships among the evaluated pairs and confirms the patterns summarized in Table 2. In the SWOT–AWAC panel, the point cloud is concentrated along the line of identity, reflecting a correlation value of approximately 0.94. The estimated regression slope is close to 1.06, and the intercept is about 0.14, indicating a moderate tendency for SWOT to record slightly higher heights than those measured by AWAC. The RMSE remains approximately 0.25 m, indicating good agreement at the observed scale. In the SWOT–WW3 panel, the relationship remains consistent, featuring a correlation of around 0.88 and a slope of nearly 1.01, while the intercept is approximately –0.19. In the AWAC–WW3 panel, the correlation is around 0.90, the slope is about 1.16, and the intercept is approximately –0.15.

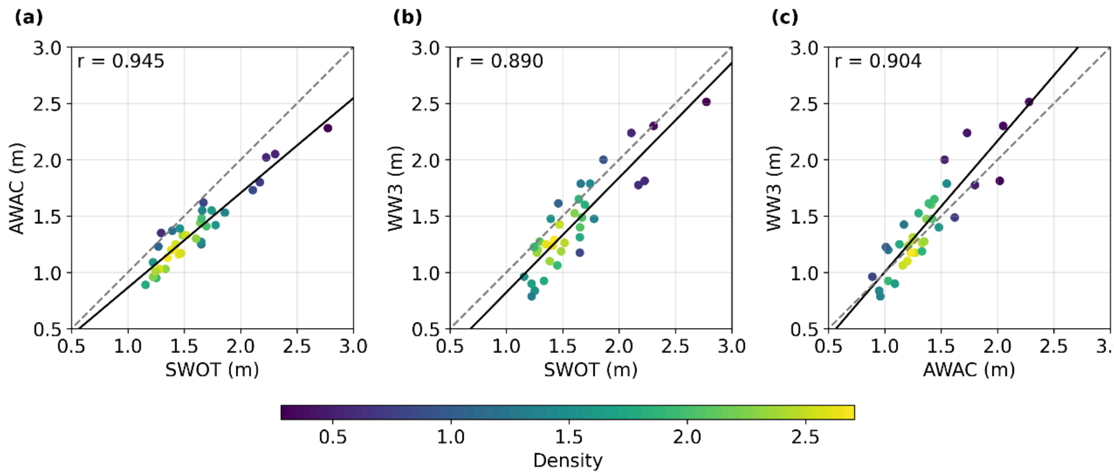

Figure 4. Scatter plots of SWH and linear fits for the three pairwise comparisons: (a) SWOT vs AWAC, (b) SWOT vs WW3, (c) AWAC vs WW3. Grey markers are the data points; the solid black line is the linear regression (ordinary least squares) fitted to each pair, and the black dashed line is the 1:1 reference. Each panel displays the Pearson correlation coefficient (R) for that pair. All reported correlations are significant at $p < 0.001$.

Although the AWAC–WW3 comparison exhibits the smallest RMSE, the strong agreement between SWOT and AWAC confirms the ability of SWOT to reproduce the observed wave conditions. The consistency between SWOT and WW3 further indicates that the satellite observations are coherent with the large-scale wave patterns represented by the model. The proximity between the fitted lines and the line of identity reinforces the consistency among the three pairwise comparisons. Collectively, the three plots demonstrate that the numerical results presented in Table 2 are clearly reflected in each pairwise comparison (SWOT–AWAC, SWOT–WW3, and AWAC–WW3).

DISCUSSION

The results of this study show high agreement among the compared series. The Pearson correlation between SWOT and AWAC was approximately 0.94, with a mean bias of −0.23 m, indicating that SWOT underestimated AWAC, and an RMSE of 0.25 m. The correlation between SWOT and WW3 was about 0.88, with a mean bias of +0.17 m, indicating that SWOT overestimated WW3, and an RMSE of 0.24 m. Between AWAC and WW3, the correlation was near 0.90, with a mean bias of −0.06 m, indicating that AWAC slightly underestimated WW3, and an RMSE of 0.19 m. In relative terms, the normalized mean bias was −16.90% for SWOT–AWAC, +10.44% for SWOT–WW3, and −4.70% for AWAC–WW3, confirming the same overall pattern observed in the absolute error metrics. These values are consistent with validation results for conventional altimetry in open-ocean regions: for example, in an assessment of the Sentinel-3 mission against NDBC buoys, an RMSE of approximately 0.30 m and bias magnitudes ranging from centimeters to tenths of a meter were reported (Yang & Zhang, 2019). This agreement with the literature suggests that SWOT performance, even with limited point samples, is compatible with accepted standards for altimetric SWH products.

The close correspondence between SWOT-derived SWH and AWAC observations is consistent with previous altimeter validation studies conducted in coastal and open-ocean environments, which report typical RMSE values of 0.20–0.40 m for comparisons against buoys and acoustic sensors (Queffeulou, 2004). Furthermore, the agreement between SWOT and WW3 suggests that the satellite-derived wave fields are physically consistent with the broader regional wave conditions represented by the numerical model. Modest inter-platform discrepancies are commonly ascribed not to the sensor family per se but to differences in instrumental footprint, retracker algorithms, and spatial representativeness, factors that become particularly consequential in coastal regions exhibiting strong spatial gradients and heterogeneous wave fields. Such representativeness errors can persist even when correlation coefficients are high. Moreover, validations using higher spatial-resolution altimeters (e.g., HY-2B) have shown reductions in coastal biases and improved agreement with in-situ measurements in confined and near-shore waters (Hong et al., 2022), thereby reinforcing the coherence observed in the present study.

The SWOT mission provides a key advantage over conventional nadir altimeters: its ability to map the ocean surface in two dimensions, potentially capturing swells and spatial heterogeneities in the wave field that would not be detected by a buoy or a single altimetric ground track. This capability may partly explain the coexistence of high correlation with localized biases and pointwise dispersion among the series. Recent studies using multi-mission altimetry and SWOT have shown that the combination of altimetric passes can resolve more than 75% of storm events and capture approximately 80% of the spatial variability of coastal and open-ocean waves (Turki et al., 2025). These findings reinforce that, despite temporal sampling limitations, SWOT has strong potential to complement buoys and models from a more spatially comprehensive perspective.

The limitations of the present study are evident and should be regarded. The time series is short (slightly longer than one month) due to the restricted temporal overlap between the satellite overpasses and the periods during which the in situ instrument (AWAC) was operating close enough for comparison. This reduces the statistical robustness for capturing extreme events, seasonal variability, and infrequent localized effects. The literature notes that spatial representativeness, temporal collocation windows, and location-matching criteria can significantly affect validation metrics (bias, RMSE, correlation) in SWH altimetry studies, particularly in coastal or transitional regions where spatial heterogeneity is more pronounced (e.g., Queffeulou et al., 2004; Broad-scale altimeter validation). Moreover, the inclusion of the global WW3 product as a spatially continuous model field provides useful regional context; however, global models generally lose detail at local or coastal scales, where higher-resolution regional models may provide superior performance. This suggests that future comparisons should incorporate regional modeling systems and possibly specialized coastal retrackers for altimetry. Although SWOT has the potential to capture swells and spatial heterogeneities in the wave field, this aspect was not explored here because the present study was designed as a point-based validation of SWOT-derived SWH against AWAC observations. WW3 was included only as an auxiliary numerical field for spatial context, under limited temporal overlap and collocated matchup conditions. A dedicated spatial analysis of the SWOT swath and its comparison with model fields is therefore left for future work.

To advance this line of research, we recommend expanding the analysis beyond wave height alone. Including the validation of parameters such as dominant period and wave direction, as well as employing spectral analysis techniques (e.g., fast Fourier transform, wavelet analysis), could reveal discrepancies that depend on the spectral distribution of wave energy, features not captured by pointwise SWH metrics. Recent studies have shown that machine-learning approaches applied to multi-source altimetry and buoy datasets can significantly reduce bias and scatter in wave estimates (e.g., Qian et al., 2025; Yang et al., 2025). The adoption of such methodologies in contexts like the present study could enhance the reliability and applicability of SWOT-derived products.

CONCLUSIONS

The present study demonstrated that the SWH estimates derived from the SWOT mission exhibit high temporal and statistical consistency with AWAC wave gauge measurements, which served as the independent reference dataset on the continental shelf near the Abrolhos Archipelago. The consistency between SWOT and WW3 outputs further supports the physical coherence of the satellite-derived wave fields at the regional scale. The series showed high correlations (R ≈ 0.90) and mean errors within the expected range for coastal altimetry validations. Although a moderate systematic bias was observed in the SWOT estimates throughout the time series, the results confirm that the SWOT SWH product is robust for spatial monitoring applications in continental shelf environments.

Despite the limitations of the present work, mainly the short temporal window available for comparison, the study provides valuable findings. It corroborates the quality of SWOT SWH data on the continental shelf, demonstrating that the mission can complement direct measurements by providing a spatially continuous description of the wave field in coastal studies and wave monitoring applications.

ACKNOWLEDGMENTS

We thank the managers and crew of the R/V Ciências do Mar IV for their contribution to the success of the operations during the cruises, as well as the students and professors of DOCEAN-UFPE. This research was carried out in collaboration with ANR–FACEPE through the SargAlert project (grant number APQ-0411-1.08/22) and with FACEPE through the NOPE project (grant number APQ-0235-1.08/23). The author A.C.S. gratefully acknowledges the Brazilian funding agency CNPq (National Council for Scientific and Technological Development) for its financial support. This work is a contribution to the International Joint Laboratory TAPIOCA (www.tapioca.ird.fr).

AUTHOR CONTRIBUTION

Y.O.P: Conceptualization; Methodology; Investigation; Writing – original draft; Writing – review & editing.

A.C.S.: Methodology; Investigation; Writing – review & editing.

R.V.A.: Methodology; Investigation; Writing – review & editing.

G.D.G.: Methodology; Investigation; Writing – review & editing.

M.S.: Methodology; Investigation; Writing – review & editing.

A.L.: Methodology; Investigation; Writing – review & editing.

A.T.L.: Methodology; Investigation; Writing – review & editing.

F.H.: Writing – review & editing.

DATA AVAILABILITY STATEMENT

The SWOT significant wave height data used in this study are publicly available through the

AVISO+ data portal (https://www.aviso.altimetry.fr/en/data/products/windwave-products/swot-karin-level-3-wind-wave-product.html). The AWAC wave observations are not publicly available but may be obtained from the corresponding author upon reasonable request. The WW3 model data used in this study were provided by Surfguru (https://www.surfguru.com.br), whose wave forecasting system is based on the NOAA Global Forecast System and the WW3 global wave model. These data are not publicly available through the Surfguru platform but may be made available free of charge for research purposes upon formal request to the company.

CONFLICTS OF INTEREST

The authors declare no conflicts of interest.

AI USE DISCLOSURE

Artificial intelligence tools (specifically Grammarly) were used exclusively to refine the English language of the manuscript. No generative text, ideas, analyses, figures, or scientific content were produced by AI. All content was thoroughly reviewed and validated by the authors, who are fully responsible for the accuracy of the final manuscript version.

FUNDING

We acknowledge the Brazilian Navy, the company Petróleo Brasileiro S.A. (PETROBRAS), and the National Petroleum Agency (ANP) for making the work on board possible through the SIGITEC Cooperation Terms 2018/00451-6 and 2018/00452-2

REFERENCES

Ardhuin, F., Molero, B., Bohé, A., Nouguier, F., Collard, F., Houghton, I., Hay, A. & Legresy, B. 2024. Phase-Resolved Swells Across Ocean Basins in SWOT Altimetry Data: Revealing Centimeter-Scale Wave Heights Including Coastal Reflection. Geophysical Research Letters, 51(16), e2024GL109658. DOI: https://doi.org/10.1029/2024GL109658

Castro, B. M., Dottori, M. & Pereira, A. F. 2013. Subinertial and tidal currents on the Abrolhos Bank shelf. Continental Shelf Research, 70, 3–12. DOI: https://doi.org/10.1016/j.csr.2013.09.025

Cotrim, C. D. S., Semedo, A. & Lemos, G. 2022. Brazil Wave Climate from a High-Resolution Wave Hindcast. Climate, 10(4), 53. DOI: https://doi.org/10.3390/cli10040053

Fu, L.-L. & Ubelmann, C. 2014. On the Transition from Profile Altimeter to Swath Altimeter for Observing Global Ocean Surface Topography. Journal of Atmospheric and Oceanic Technology, 31(2), 560–568. DOI: https://doi.org/10.1175/JTECH-D-13-00109.1

Guérin, A., Piras, F., Cuvillon, N., Homerin, A., Le Gac, S., Maraldi, C., Bignalet-Cazalet, F., Alves, M. &

Rey, L. 2024. Description and In-Flight Assessment of the POSEIDON-3C Altimeter of the SWOT Mission. Remote Sensing, 16(22), 4183. DOI: https://doi.org/10.3390/rs16224183

Hong, Z., Yang, J., Liu, S., Jia, Y., Fan, C. & Cui, W. 2022. Coastal Waveform Retracking for HY-2B Altimeter Data by Determining the Effective Trailing Edge and the Low Noise Leading Edge. Remote Sensing, 14(19). DOI: https://doi.org/10.3390/rs14195026

Instituto Chico Mendes de Conservação da Biodiversidade. 2018. Plano Interpretativo: Parque Nacional Marinho dos Abrolhos (p. 70). Brasília. Retrieved from https://www.gov.br/icmbio/pt-br/assuntos/biodiversidade/unidade-de-conservacao/unidades-de-biomas/marinho/lista-de-ucs/parna-marinho-dos-abrolhos/downloads/plano_interpretativo_pnmabrolhos_2018.pdf

Knoppers, B., Ekau, W. & Figueiredo, A. G. 1999. The coast and shelf of east and northeast Brazil and material transport. Geo-Marine Letters, 19(3), 171–178. DOI: https://doi.org/10.1007/s003670050106

Lessa, G. C. & Cirano, M. 2006. On the circulation of a coastal channel within the Abrolhos Coral-Reef System - Southern Bahia (17°40'S), Brazil. Journal of Coastal Research, SI 39, 450–453.

López-García, P., Gómez-Enri, J. & Muñoz-Pérez, J. J. 2019. Accuracy assessment of wave data from altimeter near the coast. Ocean Engineering, 178, 229–232. DOI: https://doi.org/10.1016/j.oceaneng.2019.03.009

Mahadevan, A. 2016. The Impact of Submesoscale Physics on Primary Productivity of Plankton. Annual Review of Marine Science, 8(1), 161–184. DOI: https://doi.org/10.1146/annurev-marine-010814-015912

Marinha do Brasil. 2025. WAVEWATCH III. Accessed: https://www.marinha.mil.br/chm/pagina-basica/wavewatch-iii

Morete, M. E., Marques, M. L., De Souza, R. C. F., Tristão, I. A., Motta, M. C., Martins, C. C. A., Cardoso, J. & Francisco, A. 2022. Is the reproductive area of the humpback whale (Megaptera novaeangliae) in Brazilian waters increasing? Evidence of breeding and calving activities around Ilhabela, São Paulo, Brazil. Latin American Journal of Aquatic Mammals. DOI: https://doi.org/10.5597/lajam00281

NOAA. 2025. The WAVEWATCH III Development Group. Accessed: https://polar.ncep.noaa.gov/waves/wavewatch/

Pianca, C., Mazzini, P. L. F. & Siegle, E. 2010. Brazilian offshore wave climate based on NWW3 reanalysis. Brazilian Journal of Oceanography, 58(1), 53–70. DOI: https://doi.org/10.1590/S1679-87592010000100006

Queffeulou, P. 2004. Long-Term Validation of Wave Height Measurements from Altimeters. Marine Geodesy, 27(3–4), 495–510. DOI: https://doi.org/10.1080/01490410490883478

Qian, C., Zhang, Z., Ou, Y. & Jiang, H. 2025. Multi-source calibration of wind speed and wave height from altimeter by machine learning. Intelligent Marine Technology and Systems, 3(1), 21. DOI: https://doi.org/10.1007/s44295-025-00073-4

Surface Water and Ocean Topography (SWOT) Project. 2024. Release note: SWOT version C KaRIn science data products. JPL/NASA. Retrieved from https://podaac-www.jpl.nasa.gov/announcements/2024-03-06-SWOT-KaRIn-Science-Data-Products-Release

Teixeira, C. E. P., Lessa, G. C., Cirano, M. & Lentini, C. A. D. 2013. The inner shelf circulation on the Abrolhos Bank, 18°S, Brazil. Continental Shelf Research, 70, 13–26. DOI: https://doi.org/10.1016/j.csr.2013.09.003

Timmermans, B. W., Gommenginger, C. P., Dodet, G. & Bidlot, J. -R. 2020. Global Wave Height Trends and Variability from New Multimission Satellite Altimeter Products, Reanalyses, and Wave Buoys. Geophysical Research Letters, 47(9), e2019GL086880. DOI: https://doi.org/10.1029/2019GL086880

Tolman, H. L. 1989. The numerical model WAVEWATCH: a third generation model for hindcasting of wind waves on tides in shelf seas (Technical Report No. Report No. 89-2). Delft, Netherlands: Delft University of Technology.

Tolman, H. L. 1991. A Third-Generation Model for Wind Waves on Slowly Varying, Unsteady, and Inhomogeneous Depths and Currents. Journal of Physical Oceanography, 21(6), 782–797.

Tolman, H. L. 1992. Effects of Numerics on the Physics in a Third-Generation Wind-Wave Model. Journal of Physical Oceanography, 22(10), 1095–1111.

Tolman, H. L. 1997. User manual and system documentation of WAVEWATCH-III version 1.15 (Technical Note No. OMB Contribution No. 151). Washington, DC: NOAA/NWS/NCEP.

Tolman, H. L. 1999a. User manual and system documentation of WAVEWATCH-III version 1.18 (Technical Note No. OMB Contribution No. 166). Washington, DC: NOAA/NWS/NCEP.

Tolman, H. L. 2002. User manual and system documentation of WAVEWATCH-III version 2.22 (Technical Note No. MMAB Contribution No. 222). Washington, DC: NOAA/NWS/NCEP.

Tolman, H. L. 2009. User manual and system documentation of WAVEWATCH III version 3.14 (Technical Note No. MMAB Contribution No. 276). Camp Springs, MD: NOAA/NWS/NCEP.

Turki, E. I., Salameh, E., Lopez Solano, C., Islam, M. S., Domingues, M., Aouf, L., Gutierrez, D., Carbonnière, A. & Frappart, F. 2025. Multi-Source Satellite Altimetry for Monitoring Storm Wave Footprints in the English Channel's Coastal Areas. Remote Sensing, 17(18), 3262. DOI: https://doi.org/10.3390/rs17183262

Wang, J. & Fu, L.-L. 2019. On the Long-Wavelength Validation of the SWOT KaRIn Measurement. Journal of Atmospheric and Oceanic Technology, 36(5), 843–848. DOI: https://doi.org/10.1175/JTECH-D-18-0148.1

Wang, J., Fu, L.-L., Qiu, B., Menemenlis, D., Farrar, J. T., Chao, Y., Thompson, A. F. & Flexas, M. M. 2018. An Observing System Simulation Experiment for the Calibration and Validation of the Surface Water Ocean Topography Sea Surface Height Measurement Using In Situ Platforms. Journal of Atmospheric and Oceanic Technology, 35(2), 281–297. DOI: https://doi.org/10.1175/JTECH-D-17-0076.1

Yang, J. & Zhang, J. 2019. Validation of Sentinel-3A/3B Satellite Altimetry Wave Heights with Buoy and Jason-3 Data. Sensors, 19(13), 2914. DOI: https://doi.org/10.3390/s19132914

Yang, S., Zhang, L., Peng, H., Zhou, W., Song, Q., Mu, B. & Zhang, Y. 2025. Representativeness Error Assessment and Multi-Method Scaling of HY-2B Altimeter Significant Wave Height. Remote Sensing, 17(23). DOI: https://doi.org/10.3390/rs17233829

Zhang, H., Fan, C., Sun, L. & Meng, J. 2024. Study of the ability of SWOT to detect sea surface height changes caused by internal solitary waves. Acta Oceanologica Sinica, 43(5), 54–64. DOI: https://doi.org/10.1007/s13131-024-2324-9